Supporting Information

Dual Internal Electric Field Synergistic Interface and Surface Modification Enhances Photoelectrochemical Performance of Hematite Photoanodes

Shanshan Jiang[a], Lina Ding[c], Dabo Liu[a], Guanya Wang[a], Ran Tao[a, b], Zhenming Chu[a, b] Xiaoxing Fan[a, b*] and Jie Guan[c*]

[a] *School of Physics, Liaoning University, Shenyang, 110036. P. R. China.*
[b] *Liaoning Key Laboratory of Semiconductor Light Emitting and Photocatalytic Materials, Liaoning University, Shenyang 110036, P. R. China.*
[c] *Key Laboratory of Quantum Materials and Devices of Ministry of Education, School of Physics, Southeast University, Nanjing, 211189, P. R. China.*

[*] Corresponding author.
E-mail address: xxfan@lnu.edu.cn (XX. Fan), guanjie@seu.edu.cn (J. Guan)

1. Additional Experimental section

1.1. Characterization equipment

Morphologies of Fe_2O_3-based thin films were characterized with a scanning electron microscope (SEM, Regulus 8100) and a transmission electron microscope (TEM, JEOL, JEM-2100F). Structural and crystallinity properties of the prepared thin films were investigated using a Tongda TD-3500 X-ray diffraction (XRD) system in a 2θ range of 5°~80° (C1u Ka). The element composition and chemical states were studied by a Thermo Scientific ESCALAB Xi+ Probe spectrometer with a monochromatic AlKα source (photon energy 1486.68 eV), a spot size of 400 μm, pass energy of 100 eV, and energy step size of 1.0 eV. Optical properties of photoelectrodes were measured with a UH4150 Spectrophotometer UV-Vis-NIR model. UPS was performed by PHI 5000 VersaProbe III with He I source (21.22 eV) under an applied negative bias of 9.0 V. The separation and kinetic behaviors of photogenerated charge carriers were studied with the aid of lock-in-based SPV measurements (300-800 nm). The gas evolution was analyzed by gas chromatography (GC1690, JieDao) with a three-electrode system at 1.23 V_{RHE}.

1.2. Photoelectrochemical measurements

A standard three-electrode system was used for measuring the PEC performance on an electrochemical workstation (Princeton Applied Research 2273) including Pt as a counter electrode, Ag/AgCl as a reference electrode, and Fe_2O_3-based photoanodes as working electrodes. The PEC performance was measured under 100 mW cm^{-2} (AM 1.5G) on the back-side of photoelectrodes. Light irradiated into 1 cm^2 of photoanode which immersed in the 1 M KOH electrolyte. In order to measure Electrochemical impedance spectroscopy (EIS) the frequency varied from 10 kHz to 0.1 Hz.

2. The equations

Eq S1 was used to convert Ag/AgCl reference potential into **RHE:**[1]

$$V_{RHE} = V_{Ag/Agcl} + 0.197 + 0.059\,pH \qquad \text{S1}$$

Eq S2 was used to calculate **IPCE:**[2]

$$IPCE = \frac{J \times 1240}{\lambda \times P_{light}} \times 100\% \qquad \text{S2}$$

Where J is the photocurrent density (mA cm^{-2}); λ is the incident light wavelength (nm); P_{light} is the power density (mW cm^{-2}).

Eq S3 was used to calculate **ABPE:**[3]

$$ABPE = \frac{J(1.23 - V_b)}{P} \times 100\% \qquad \text{S3}$$

where J is the photocurrent density of samples, V_b is the applied external potential *vs.* RHE and P_{light} is the power density of the illumination (100 $mWcm^{-2}$).

Eq S4 was used to calculate **H_2&O_2 evolution:**[4]

$$H_2(or\ O_2)\mu mol.cm^{-2} = \left(\frac{Area\ of\ H_2(or\ O_2)peak}{Slope\ of\ calibration\ curve\ for\ H_2(or\ O_2)}\right) \times (Head\ space\ volume) \times \left(\frac{1mol}{24.2\ L}\right) \qquad \text{S4}$$

Eq S5 was used to calculate **J_{abs}:**[5]

$$J_{abs} = \frac{q}{hc}\int_{\lambda}^{\lambda_2} \lambda \phi_{\lambda} \eta_{abs} d\lambda \qquad \text{S5}$$

Where h was the Plank constant, c was the light speed, ϕ_λ was the photon flux of the AM 1.5G solar spectrum, and η_{abs} was the light absorption efficiency.

Eq S6 was used to calculate η_{sep}[6]

$$\eta_{sep} = \frac{J_{Na_2SO_3}}{J_{abs}} \qquad \text{S6}$$

Where The $J_{Na_2SO_3}$ was the photocurrent density measured in 1 M KOH and0.5 M Na_2SO_3 mixed electrolyte, which served as hole scavengers to ensure the hole injection rate approaching 100%.

Eq S7 was used to calculate η_{inj}:[7]

$$\eta_{inj} = \frac{J_{H_2O}}{J_{Na_2SO_3}} \qquad \text{S7}$$

Where J_{H_2O} was the photocurrent densities measured in 1 M KOH.

The surface recombination rate constant (***K_{rec}***) and charge transfer rate constant (***K_{ct}***) were estimated using the given equations:[8]

$$K_{ct} = \frac{1}{R_2 CPE_2} \qquad \text{S8}$$

$$\frac{K_{rec}}{K_{ct}} = \frac{R_2}{R_1} \qquad \text{S9}$$

The charge transfer efficiency (***η_{CT}***) at the SEI is measured through the following equation:

$$\eta_{CT} = \frac{K_{ct}}{K_{ct} + K_{rec}} \qquad \text{S10}$$

3. Supplementary Figures

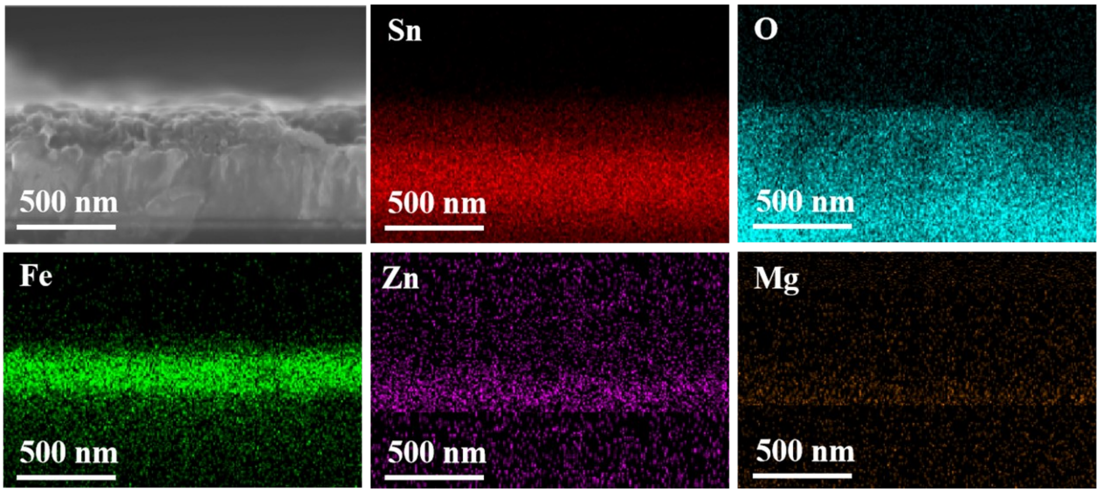

Fig. S1 Mapping of ZMO/ZT-H photoanodes.

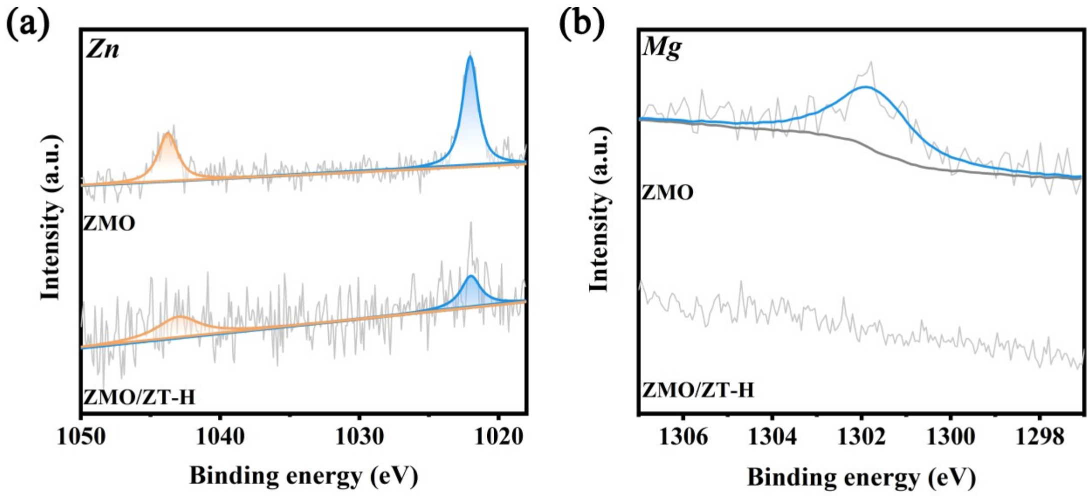

Fig. S2 XPS spectra for (a) Zn 2p and (b) Mg 2p of ZMO and ZMO/ZT-H films.

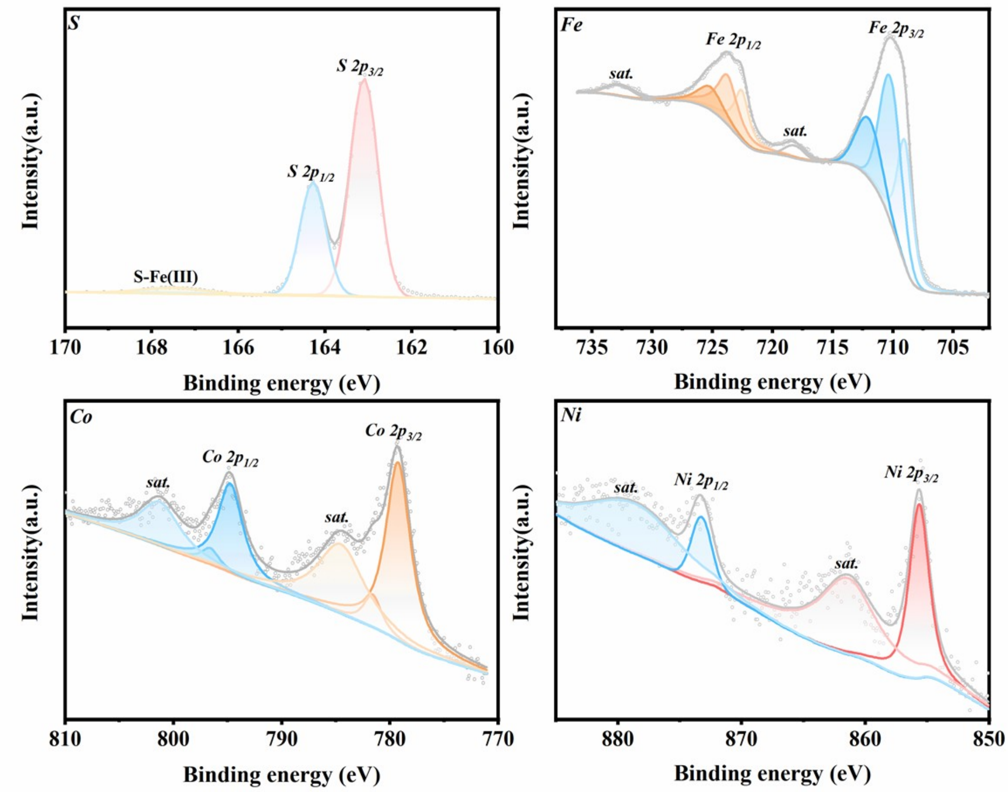

Fig. S3 XPS spectra for *S 2p*, *Fe 2p*, *Co 2p* and *Ni 2p* of ZMO/ZT-H/FS/FCN photoanodes.

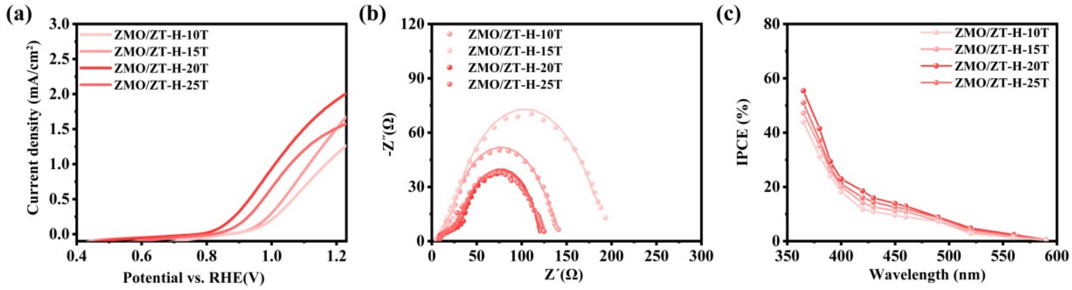

Fig. S4 (a) LSV, (b) EIS and (c) IPCE of the ZMO/ZT-H-10T, ZMO/ZT-H-15T, ZMO/ZT-H-20T and ZMO/ZT-H-25T photoanodes.

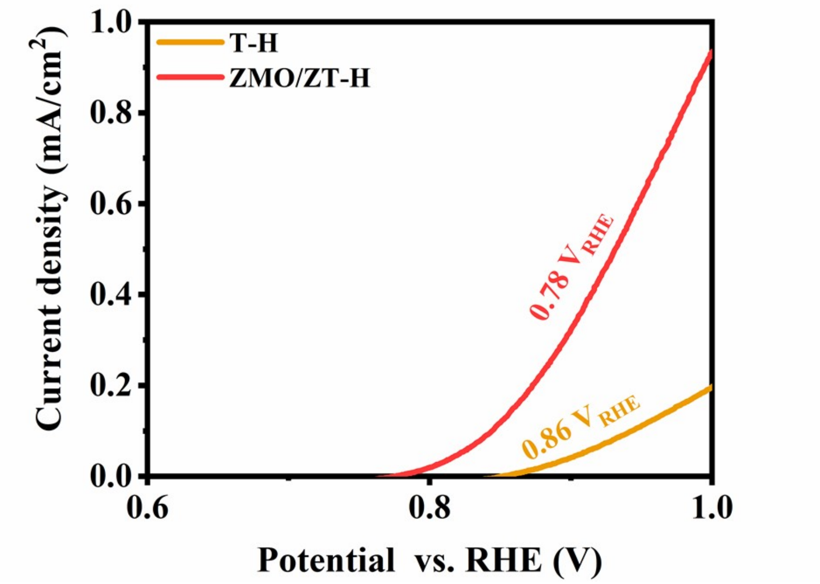

Fig. S5 Extracted V_{on} for T-H and ZMO/ZT-H photoanodes.

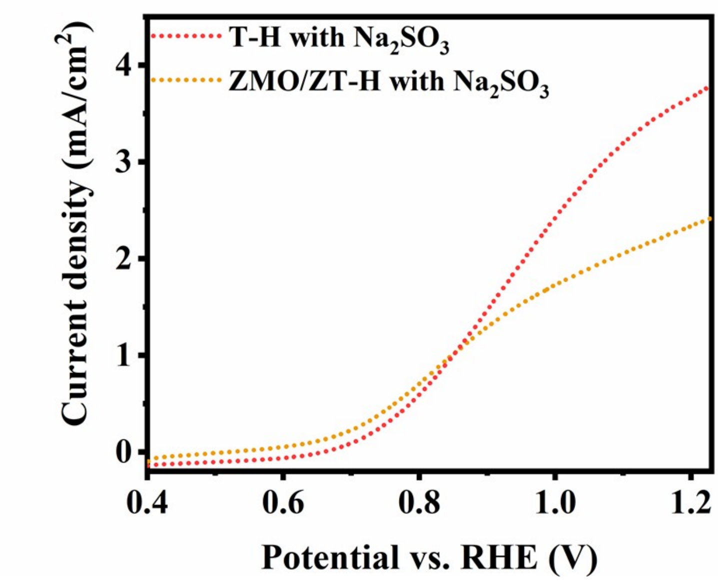

Fig S6 LSV curves of T-H and ZMO/ZT-H with the addition of Na_2SO_3.

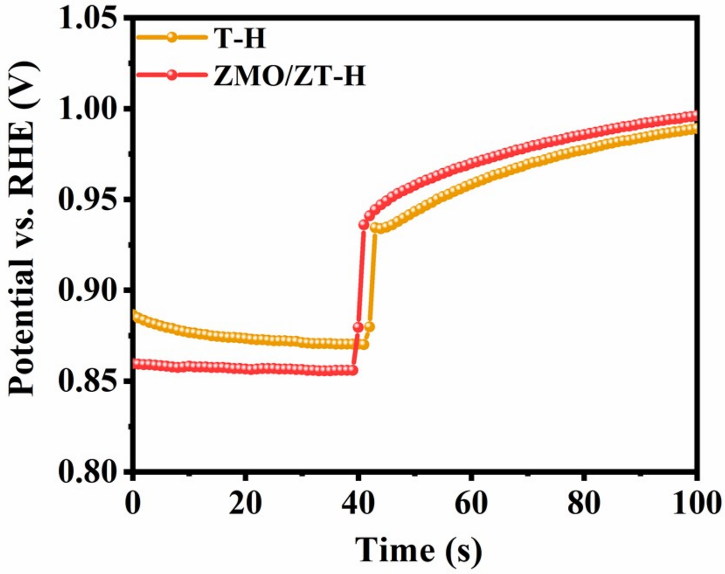

Fig. S7 OCP curves of T-H and ZMO/ZT-H photoanodes.

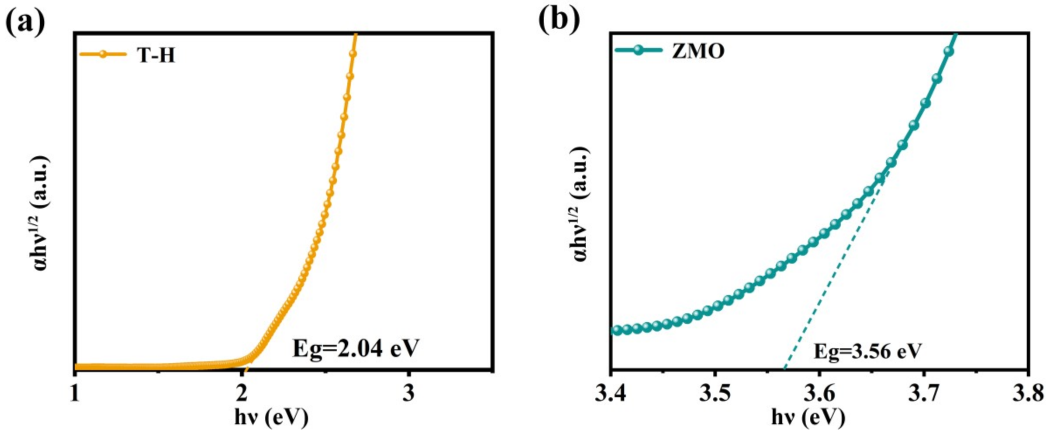

Fig. S8 Eg of (a) T-H and (b) ZMO films.

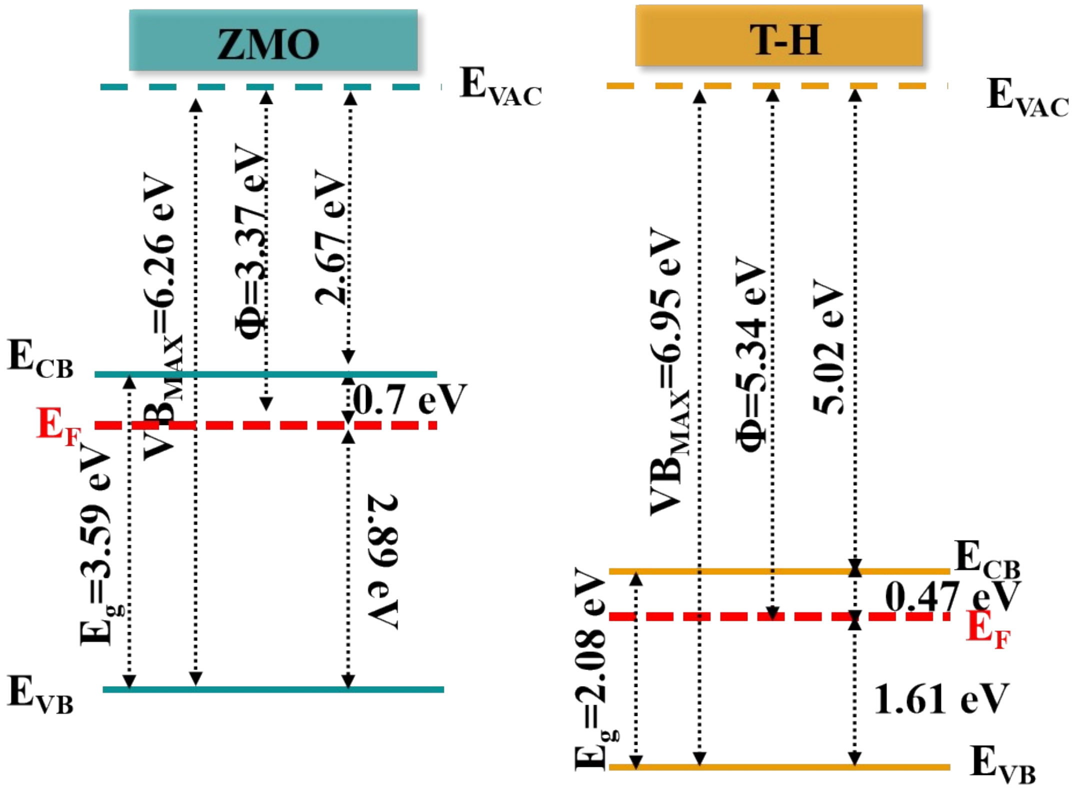

Fig. S9 Band energy diagram for (a) ZMO and (b) T-H films.

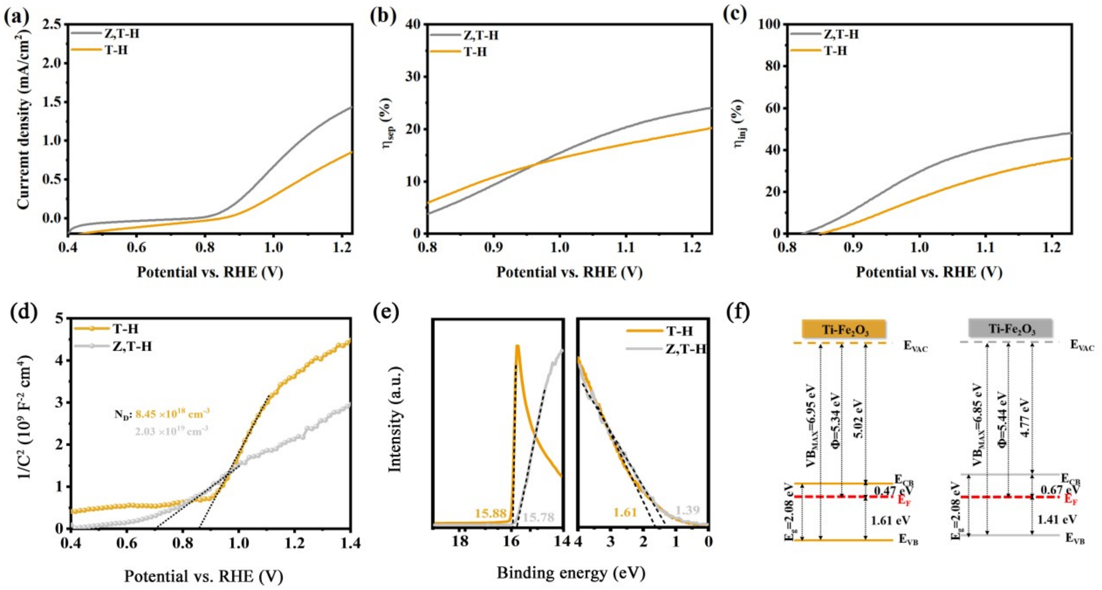

Fig. S10 (a) LSV, (b) η_{sep}, (c) η_{inj}, (d) M-S, (e) UPS and (f) band energy diagram of T-H and Z,T-H photoanodes.

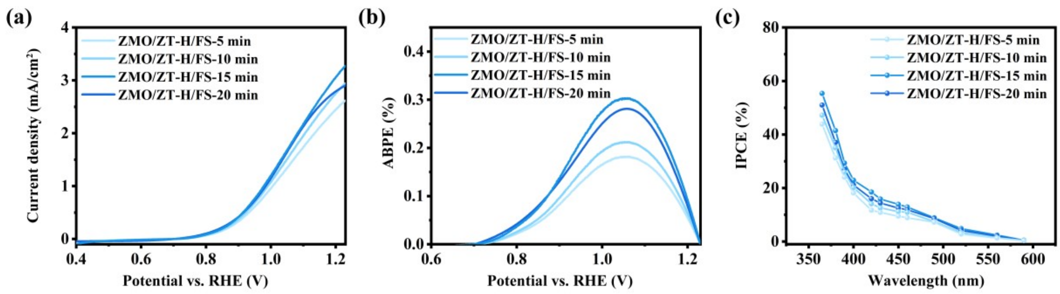

Fig. S11 (a) LSV, (b) ABPE and (c) IPCE of the ZMO/ZT-H/FS-5min, ZMO/ZT-H/FS-10 min, ZMO/ZT-H/FS-15 min and ZMO/ZT-H/FS-20 min photoanodes.

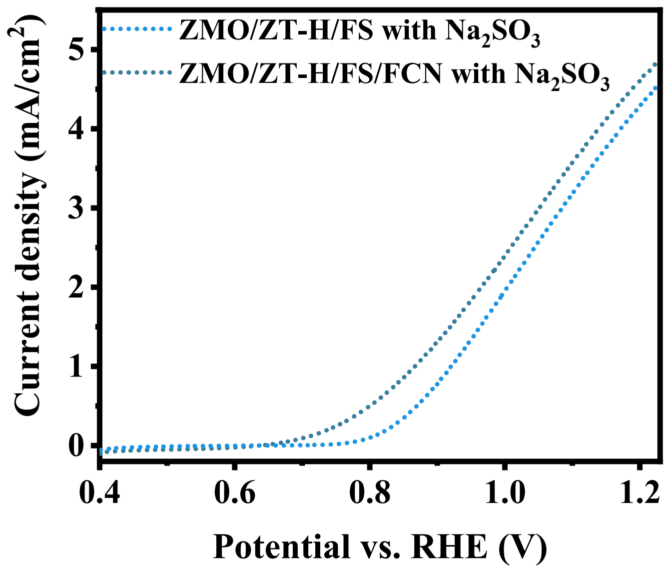

Fig. S12 LSV curves of ZMO/ZT-H/FS and ZMO/ZT-H/FS/FCN photoanodes with the addition of Na_2SO_3.

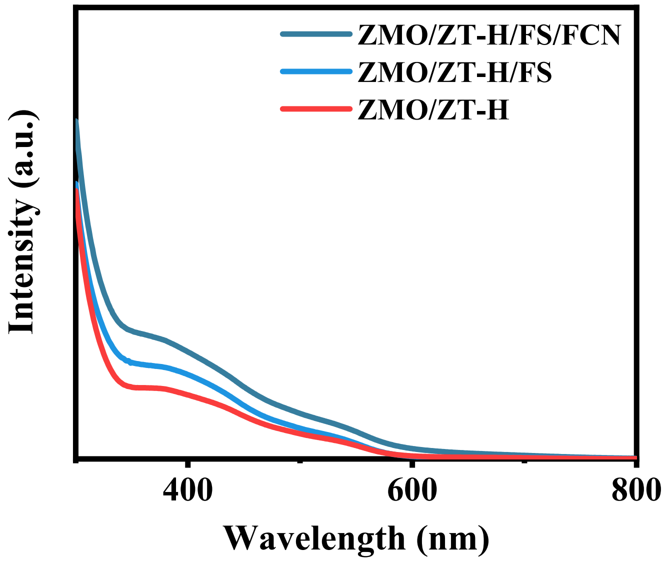

Fig. S13 UV-vis of ZMO/ZT-H, ZMO/ZT-H/FS and ZMO/ZT-H/FS/FCN photoanodes.

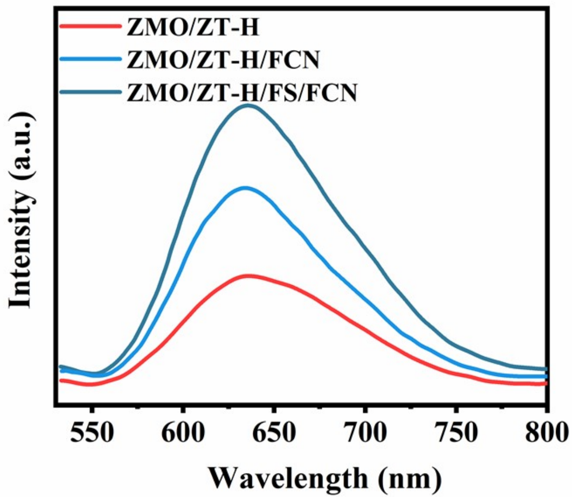

Fig. S14 PL spectra of ZMO/ZT-H, ZMO/ZT-H/FS and ZMO/ZT-H/FS/FCN photoanodes.

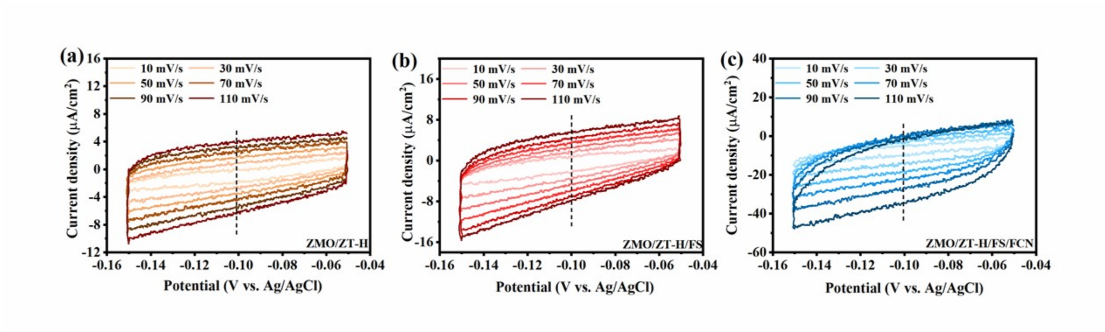

Fig. S15 high frequency EIS curves of (a) ZMO/ZT-H, (b) ZMO/ZT-H/FS and (c) ZMO/ZT-H/FS/FCN photoanodes.

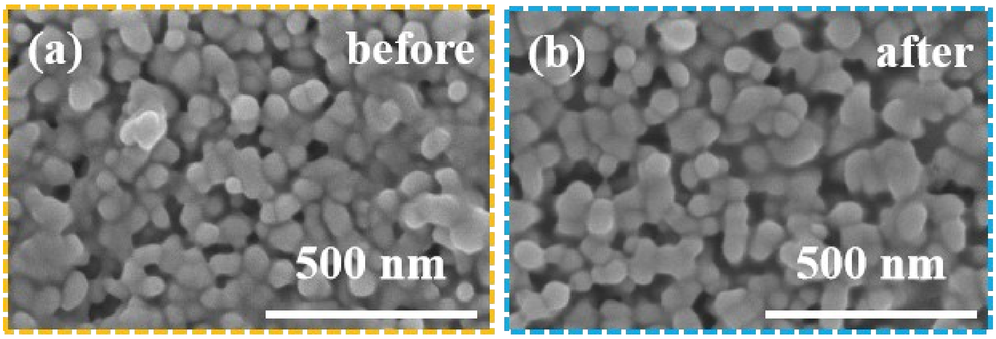

Fig. S16 SEM images of ZMO/ZT-H/FS/FCN photoanode (a) before and (b) after long-term *J-t* test.

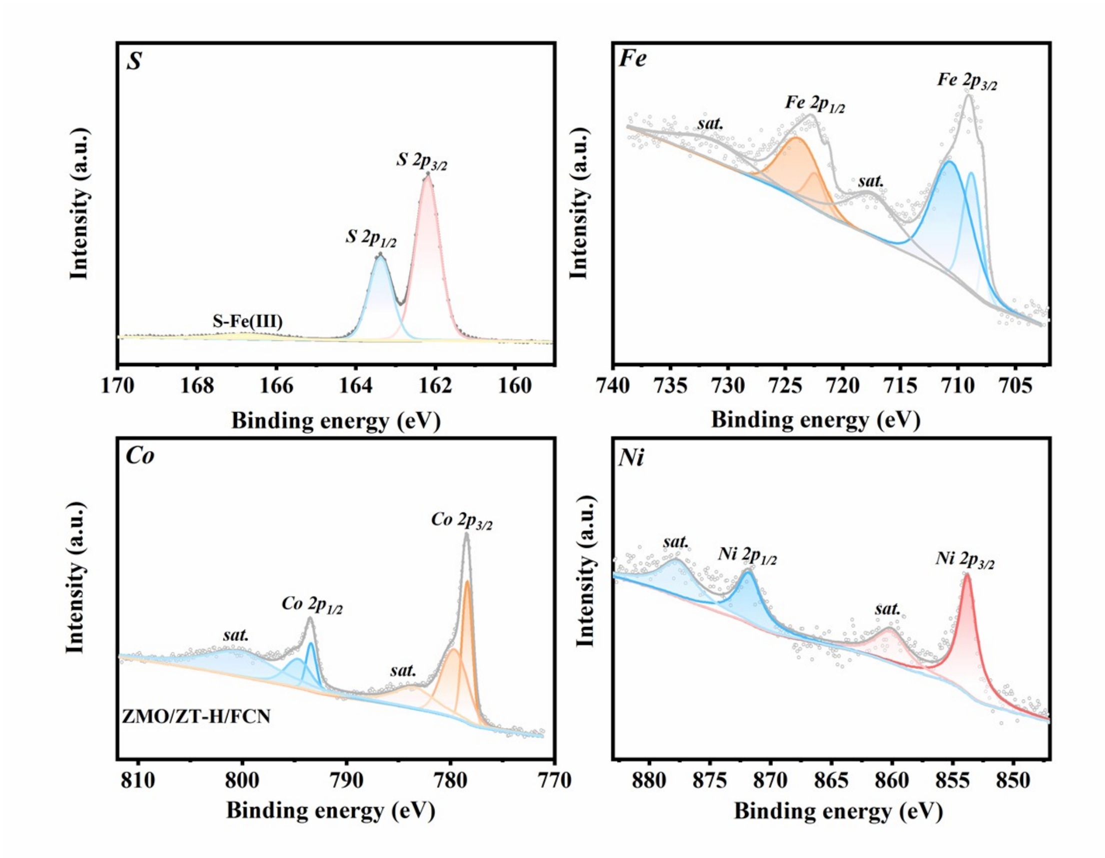

Fig. S17 XPS of ZMO/ZT-H/FS/FCN photoanode after long-term *J-t* test.

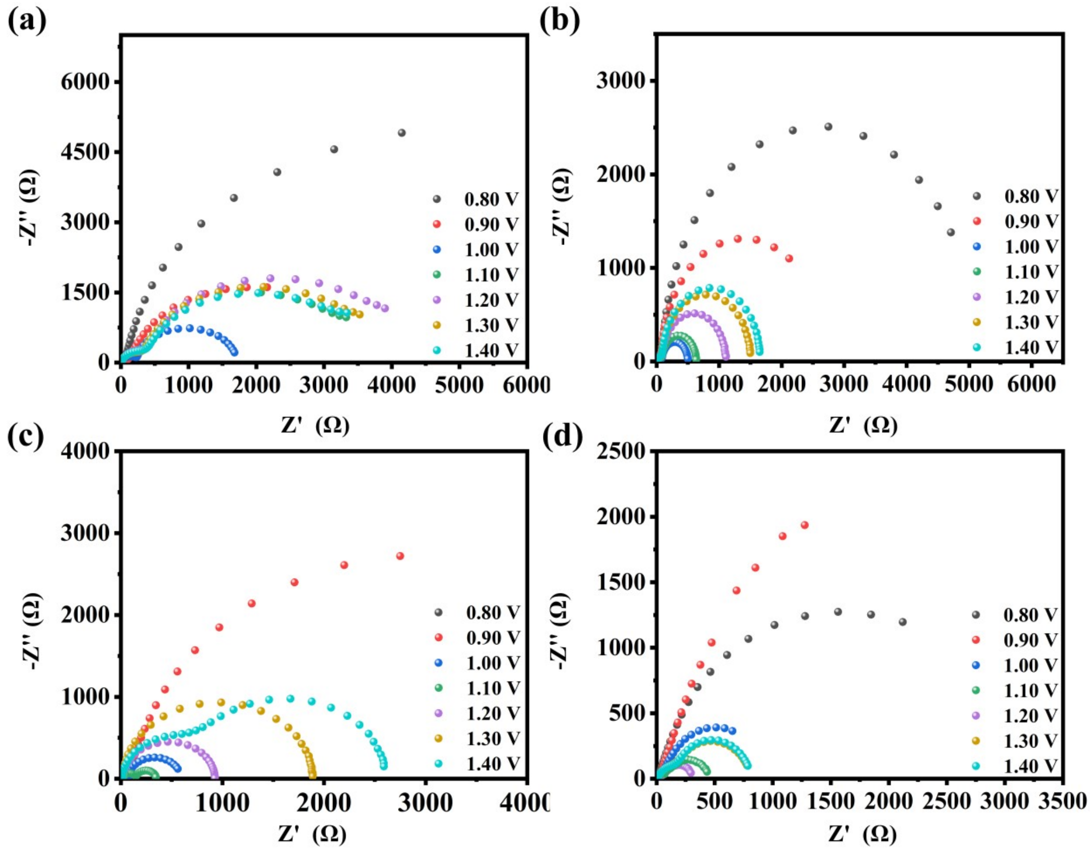

Fig. S18 PEIS curves of (a) T-H, (b) ZMO/ZT-H, (c) ZMO/ZT-H/FS and (d) ZMO/ZT-H/FS/FCN photoanodes.

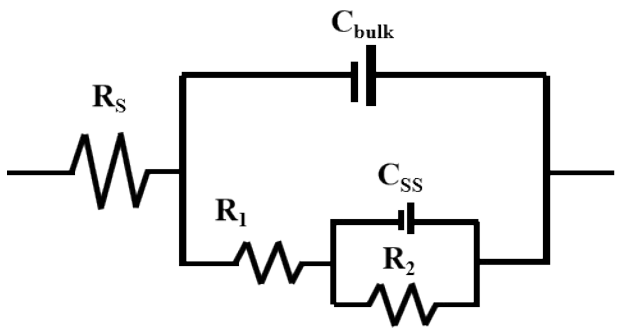

Fig. S19 Nyquist plots fitted circuit model.

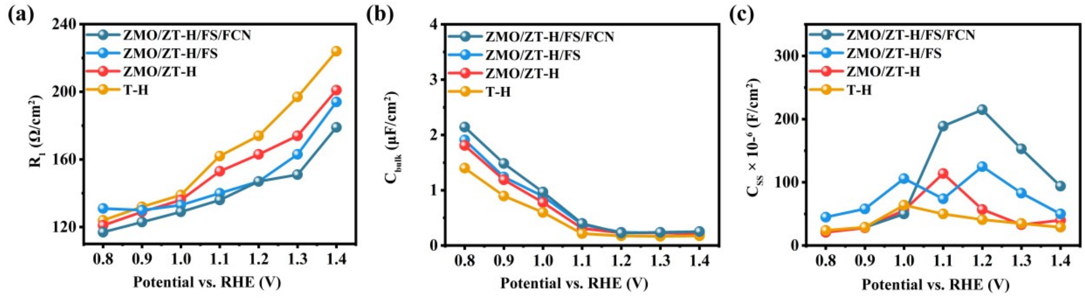

Fig. S20 R_s is the series resistance, R_1 and C_{bulk} denote the bulk charge transfer resistance and capacitance, respectively, and R_2 and C_{ss} represent the charge transfer resistance and capacitance at the electrode/electrolyte interface, respectively. (a) R_1, (b) C_{bulk} and (c) C_{SS} of T-H, ZMO/ZT-H, T-H/FCN and ZMO/ZT-H/FCN photoanodes.

4. Supplementary Tables

Table 1 The comparison in PEC performance of recent reports.

Photoanode	Current density ($mA\ cm^{-2}$)	Stability (h)	Reference
ZMO/ZT-H/FS/FCN	4.57	40	This work
rGO/Fe_2O_3	1.06	0.5	[9]
GCNN-CQD/Ti-Fe_2O_3	3.38	5.5	[10]
Co@MOF/Fe_2O_3	2.8	5	[11]
FeNiOOH/HEDP-Fe_2O_3/Fe_2TiO_5	3.4	3	[12]
Co-Pi/WRCN/Fe_2O_3	2.14	2	[13]
Ge:Ti-Fe_2O_3/AlOOH/NiFeOx	3.46	20	[14]
Fe_2O_3/CuO	0.68	1	[15]
Zr-HT/Ru–FeOOH/FNH	2.27	10	[16]
Zr/Hf-HT:MoO_3	2.34	10	[17]
Co_3O_4@Pt-Fe_2O_3	1.34	10	[18]
CoFe MTF/Fe_2O_3	2.95	9	[19]
α-Fe_2O_3/ZnO/CoTCPP/FeOOH	2.87	20	[20]
DASs Ru-P:Fe_2O_3	4.55	24	[21]
$ZnFe_2O_4$/Fe_2O_3-NIR	3.17	2.7	[22]
NiFe(OH)x/PSi/Ge-PH	4.57	50	[23]
NiFe(OH)x/Ge:Ti:Sn−Hhp	5.1	100	[24]

Reference

1 Y. Song, X. Zhang, Y. Zhang, P. Zhai, Z. Li, D. Jin, J. Cao, C. Wang, B. Zhang, J. Gao, L. Sun and J. Hou, *Angew. Chem. Int. Ed. Engl.*, 2022, **61**, e202200946.

2 S. Shen, S. A. Lindley, X. Chen and J. Z. Zhang, *Energy Environ. Sci.*, 2016, **9**, 2744-2775.

3 S. Ren, M. Sun, X. Guo, X. Liu, X. Zhang and L. Wang, *ACS Catal.*, 2022, **12**, 1686-1696.

4 F. Qu, X. Zhou, B. Zhang, S. Zhang, C. Jiang, S. Ruan and M. Yang, *J. Alloys Compd.*, 2019, **782**, 672-678.

5 T. Liu, W. Li, D. Z. Wang, T. Luo, M. Fei, D. Shin, M. M. Waegele and D. Wang, *Angew. Chem. Int. Ed.*, 2023, **62**, e202307909.

6 Y. Zhao, M. Duan, C. Deng, J. Yang, S. Yang, Y. Zhang, H. Sheng, Y. Li, C. Chen and J. Zhao, *Nat. Commun.*, 2023, **14**, 1943.

7 Y. Pihosh, V. Nandal, R. Shoji, R. Bekarevich, T. Higashi, V. Nicolosi, H. Matsuzaki, K. Seki and K. Domen, *ACS Energy Lett.*, 2023, **8**, 2106-2112.

8 Q. Zhao, P. Huang, D. Hu, T. Li and B. Xu, *ChemPhotoChem*, 2023, **7**, e202300013.

9 S. Shen, C. X. Kronawitter, D. A. Wheeler, P. Guo, S. A. Lindley, J. Jiang, J. Z. Zhang, L. Guo and S. S. Mao, *J. Mater. Chem.A*, 2013, **1**, 14498–14506.

10 S.-S. Yi, J.-M. Yan and Q. Jiang, *J. Mater. Chem.A*, 2018, **6**, 9839-9845.

11 Z.-Y. Wang, H.-M. Li, S.-S. Yi, M.-Z. You, H.-J. Jing, X.-Z. Yue, Z.-T. Zhang and D.-L. Chen, *Appl. Catal. B: Environ.*, 2021, **297**, 120406.

12 J. Deng, Y. Li, Y. Xiao, K. Feng, C. Lu, K. Nie, X. Lv, H. Xu and J. Zhong, *ACS Catal.*, 2022, **12**, 7833-7842.

13 H. Tan, W. Peng, T. Zhang, Y. Han, L. Yin, W. Si, J. Liang and F. Hou, *J. Phys. Chem. C*, 2021, **125**, 13273-13282.

14 C. Li, J. Xiao, H. Zhang, X. Jia, T. Xu, Z. Liu, Q. Zhao and B. Wang, *Chem. Eng. J.*, 2023, **476**, 146779.

15 J. Ma, Q. Wang, L. Li, X. Zong, H. Sun, R. Tao and X. Fan, *J. Colloid Interface Sci.*, 2021, **602**, 32-42.

16 P. Anushkkaran, W.-S. Chae, J. Ryu, S. H. Choi and J. S. Jang, *J. Mater. Chem. A*, 2024, **12**, 4702-4711.

17 P. Anushkkaran, M. A. Mahadik, W.-S. Chae, H. Hwi Lee, S. Hee Choi and J. Suk Jang, *Chem. Eng. J.*, 2023, **472**, 144998.

18 Y. Wei, A. Liao, W. Zhu, W. Hou, Y. Zhang, Y. Zheng, B. Zhou, Y. Yan, H. He, X. Zhou, Y. Zhou and Z. Zou, *Chem. Eng. J.*, 2023, **473**, 145384.

19 T. Yang, Z. W. Chen, X. Z. Yue, Q. C. Liu, S. S. Yi and Y. F. Zhu, *Adv. Funct. Mater.*, 2024, **34**, 2313767.

20 H. Xie, Y. Song, Y. Jiao, L. Gao, S. Shi, C. Wang and J. Hou, *ACS Nano*, 2024, **10**, 5712−5722.

21 L. L. R-T Gao, Y. Li, Y. Yang, J. He, X. Liu, X. Zhang, L. Wang, M. Wu, *Proc. Natl. Acad. Sci.* , 2023, **120**, e2300493120.

22 X. Hu, J. Huang, Y. Cao, B. He, X. Cui, Y. Zhu, Y. Wang, Y. Chen, Y. Yang, Z. Li and X. Liu, *Carbon Energy*, 2023, **5**, e369.

23 H.-J. Ahn, K.-Y. Yoon, M. Sung, H. Yoo, H. Ahn, B. H. Lee, J. Lee and J.-H. Jang, *ACS Energy Lett.*, 2023, **8**, 2595-2602.

24 J. Park, K.-Y. Yoon, B. G. Ghule, H. Kim and J.-H. Jang, *ACS Energy Lett.*, 2024, **9**, 3169-3176.